Available online at www.sciencedirect.com
SCIENCE DIRECT
Tetrahedron
Tetrahedron 62 (2006) 7866–7877

Solvent induced folding of conformationally bistable helical imide triads

Jacek Gawronski,* Magdalena Kaik, Marcin Kwit and Urszula Rychlewska

Department of Chemistry, A. Mickiewicz University, Grunwaldzka 6, 60780 Poznan, Poland

Received 20 January 2006; revised 24 April 2006; accepted 18 May 2006
Available online 19 June 2006

Abstract—Foldamer population of imide triads derived from (*R*,*R*)-1,2-diaminocyclohexane was studied with the use of ^{1}H NMR and CD spectroscopy, as well as computational modeling. Two stable foldamers of *C* and *S* shape, having correspondingly *M* and *P* helicity, are found to differ very little in energy. However, their interaction with the solvent results in significant shift of the equilibrium. For the interaction with aromatic solvent molecules a sandwich-type donor–acceptor model, stabilizing the *S* foldamer, is proposed. The limitations of the NMR and CD methods for studying the foldamer equilibrium in solution are discussed, pointing to the inadequacy of static computational models of CD spectra, not including the effect of rotation of the imide chromophores in the dynamic model of real molecules.

1. Introduction

Polymerization of monomers leads to macromolecules having new properties and capable of playing important roles, for example, as skeletal material of organisms or biocatalysts for the reactions in the cell (proteins), as the storage and transduction of genetic information (nucleic acids), and as the constituents of plant and animal tissues (oligosaccharides).[1] The structure and function of these highly functional biopolymers is determined to a large extent by intra- or intermolecular interactions, involving hydrogen bonding and stacking of planar aromatic (heterocyclic) rings.

In recent years, there has been increasing interest in basic studies of the structure and properties of artificial oligomers, which may or may be not directly related to the structure of biopolymers. The purpose of such studies is to uncover fundamental relationships between monomer structure (constitution, configuration) and oligomer conformation as well as its interaction with other molecules and ultimately to develop new lead structures for applications in materials science.

One of the basic themes of oligomer studies is their folding, i.e., the formation of ordered helical or non-helical structures, as well as their aggregation in solution. Ultimately the outcome of such studies would be predictability of oligomer folding and knowledge of the factors with which one could then tune their desired secondary structure. A particularly fascinating aspect of oligomer folding is programming of their helical structure.[2,3] Oligomer helical enantiodifferentiation may be achieved by cooperative interactions between subunits, leading to amplification of helical discrimination due to chiral substituents.[4]

The term foldamer has been coined to encompass a broad group of oligomers of well-defined bent/helical structure. In his manifesto[5] Gellman described foldamers as "polymers with a strong tendency to adopt a specific compact conformation". Moore et al. in their in-depth review[6] provided a more rigorous definition of a foldamer as "any oligomer that folds into a conformationally ordered state in solution, the structures of which are stabilized by a collection of noncovalent interactions between nonadjacent monomer units".

The most intensively studied foldamer types include oligoamides with unnatural peptide backbones,[7,8] either aromatic[9–12] or of β-peptidomimetic type.[13–15] Their secondary structure is primarily determined by the network of intramolecular hydrogen bonds.[16] Oligomers of this type are capable of creating nanocavities with tunable sizes.[17] Other foldamers of growing interest are helical strands based on heterocyclic oligomers[18] as well as *m*-phenylene ethynylene oligomers,[19] showing solvophobically driven π-stacking[20] and receptor properties.[21]

Heterogeneous backbone foldamers (i.e., those composed of two or more types of molecules) have, to date, received less

Keywords: Circular dichroism; *trans*-1,2-Diaminocyclohexane; Foldamers; Host–guest complexes; Imides; Dipole–dipole interactions.
* Corresponding author. Tel.: +48 61 829 1313; fax: +48 61 865 8008; e-mail: gawronsk@amu.edu.pl

0040–4020/$ - see front matter © 2006 Elsevier Ltd. All rights reserved.
doi:10.1016/j.tet.2006.05.039

attention. Prominent examples are aedaomers (*a*romatic *e*lectron *d*onor–*a*cceptor *o*ligo*mers*) in which the aromatic diimide and 1,5-dialkoxynaphthalene units are linked with chiral aminoacid derivatives. Oligomers of such structure and of sufficient length adopt well-defined pleated structures in solution, stabilized by donor–acceptor interactions.[22]

Imide triads **1a**–**1c**, **2a**–**2c** described in this paper represent a set of carefully chosen, structurally minimalistic foldamers, having all the characteristics of such molecules.[6] They are chain oligomers of aromatic imides and *trans*-1,2-diaminocyclohexane and their structure (in solution) can be described as a dynamic process, involving two stable foldamers, *C* and *S* of opposite helicity; for (*R*,*R*)-diaminocyclohexane derivatives, respectively, of *M* and *P* helicity.[23] The two diastereoisomers differ little in steric energy, as the two halves of the molecule obtained by dissection of the central diimide molecule can be considered identical (Fig. 1).

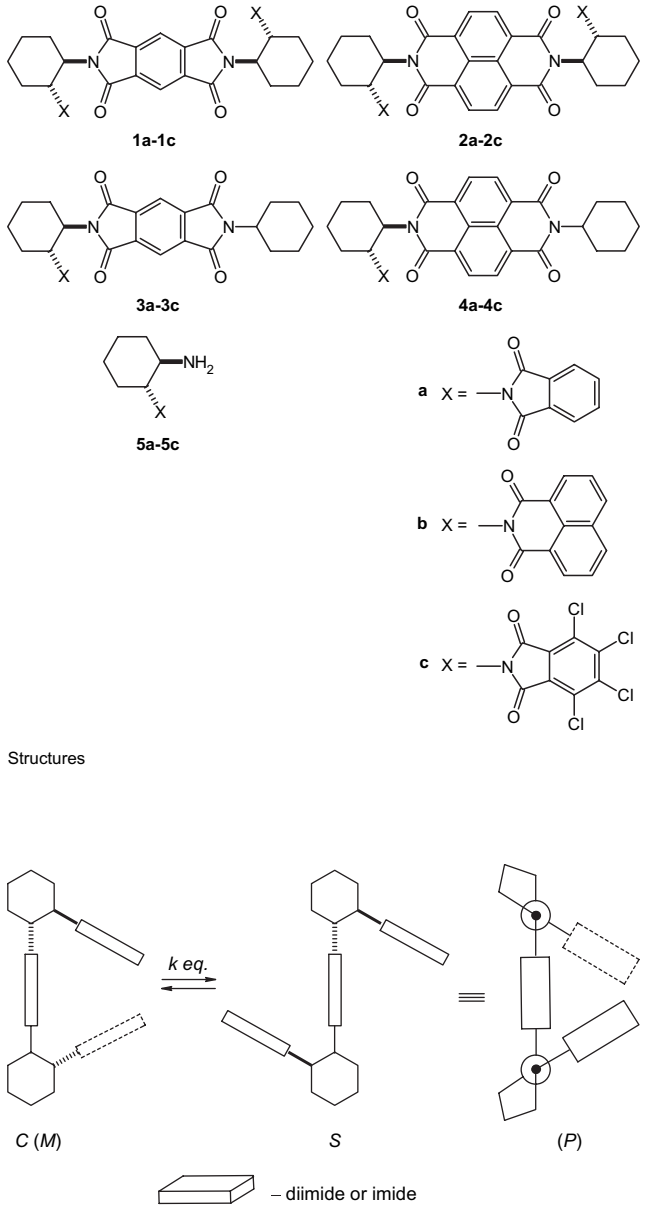

Figure 1. The two stable foldamers of imide triads with the (*R*,*R*)-1,2-diaminocyclohexane linkers.

Therefore the bistable imide triads **1a**–**1c**, **2a**–**2c** can be seen as sensitive probes for the interaction with the environment, in particular with the solvent. Although the general and important issue of foldamer stabilization by solvation has been addressed in numerous reports and accounts, much less is known about solvent effect on foldamer populations, i.e., on the role of the solvent in the folding process of a chain molecule, otherwise determined by noncovalent interactions between nonadjacent monomer units. For example, the solvent effect on conformational equilibrium of oligo(*m*-phenylene ethynylene) oligomers has been addressed by Moore[20] with the conclusion that solvent can play a dramatic role in modulating the strength of the interactions in π-stacked structures. Folding dynamics of (*m*-phenylene ethynylene)12-*mer* in various solvents has been recently analyzed by the application of Markov state model techniques.[24] Here we will show that the folding of chiral imide triads **1a**–**1c**, **2a**–**2c** can be significantly influenced by the solvent used.

2. Results and discussion

2.1. Synthesis

Imide triads **1a**–**1c**, **2a**–**2c** were obtained by condensation of 1,2,4,5-benzenetetracarboxylic dianhydride or 1,4,5,8-naphthalenetetracarboxylic dianhydride, respectively, with readily available monoprotected (*R*,*R*)-*trans*-1,2-diaminocyclohexane derivatives **5a**–**5c**.[25] We have found that the thermal condensation reaction proceeds with much higher yields (**1a**, 44%; **1c**, 48%) in refluxing acetic acid, compared to the reactions carried out in *N*,*N*-dimethylformamide at 120 °C (**1a**, 18%; **1c**, 12% yield). Dyads **3a**–**3c**, **4a**–**4c** were prepared by the condensation of monoanhydrides of either *N*-cyclohexyl-1,2,4,5-benzenetetracarboxymonoimide or *N*-cyclohexyl-1,4,5,8-naphthalenetetracarboxymonoimide,[26] respectively, with **5a**–**5c** in DMF at 120 °C, in moderate yields (32–58%).

2.2. Computational modeling

The lowest-energy structures of triads **1a**–**1c**, **2a**–**2c** as well as dyads **3a**–**3c**, **4a**–**4c** were obtained by a computational search using PM3 method, followed by DFT (b3lyp/6-31g(d)) optimization. A potential energy surface (PES) was obtained for each molecule as a function of torsion angles α_1 and α_2 (C(O)–N–CH(N)–CH_2). For example, two stable conformers, *C* and *S*, were found for triad **2b** (Fig. 2). These two low energy conformers are characterized by α_1=63°, α_2=62° and α_1=−118°, α_2=62°, respectively (Fig. 2).

In general, two stable foldamers, *C* and *S*, of close energies were obtained for each triad and one stable foldamer was found for each dyad. The common features and structural differences between these foldamers are listed in Table 1.

The foldamers of the triads can also be characterized by the dihedral angle N1–C1/C2′–N2′, involving the two outermost C–N bonds: for the *C* foldamers this angle is in the range −61 to −85° whereas it is in the range 104–122° for the *S* foldamers. *C* and *S* foldamers also differ in the

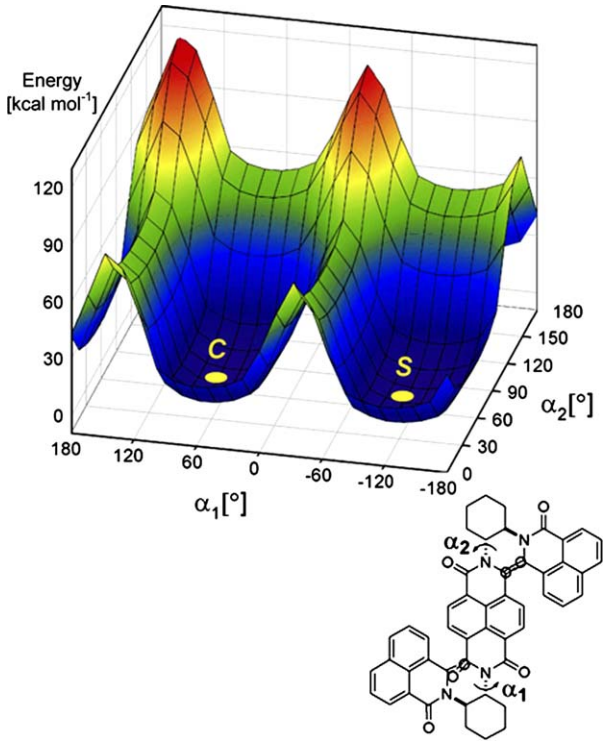

Figure 2. PM3 calculated PES and the two minima corresponding to the stable *C* and *S* conformers of **2b**.

magnitude of the computed dipole moments. The dipole moments of *C* foldamers are higher, compared to those of *S*, whereas the magnitudes of the dipole moments of *S* foldamers are slightly higher than those of the corresponding dyads. It appears that the energy differences between C and *S* conformers of imide A–B–A triads to a large extent are due to dipole–dipole interactions between the A imide components. The calculated dipole moments for *N*-methyl-1,8-naphthalenedicarboximide, *N*-methylphthalimide, and *N*-methyltetrachlorophthalimide are correspondingly 4.30 D, 2.49 D, and 0.05 D; therefore dipole–dipole interactions significantly stabilize *S* foldamers and destabilize *C* foldamers of triads **1a**, **1b**, **2a**, and **2b**. It should be noted that the energies of these dipole–dipole interactions are at the level of 0.1 kcal mol^{-1}, according to standard calculations (see Supplementary data) and can be even less significant in a high dielectric constant environment.

Table 1. Characterization of the stable foldamers of triads **1a**–**1c**, **2a**–**2c** by DFT computation (b3lyp 6-31g(d))

Triad	Foldamer	ΔE (kcal mol^{-1})	N1–C1/C2′–N2′ dihedral angle	Dipole moment (*D*)
1a	C	0.10	−73.4	3.38
	S	0.0	+110.1	2.35
1b	C	0.12	−84.8	6.06
	S	0.0	+109.8	4.09
1c	C	0.0	−66.6	0.92
	S	0.05	+104.7	0.65
2a	C	0.0	−60.7	3.40
	S	0.0	+119.2	1.98
2b	C	0.13	−61.4	6.21
	S	0.0	+117.7	3.96
2c	C	0.0	−64.9	3.90
	S	0.12	+122.5	1.89

The local conformation of the imide moieties, determined by the magnitude of the torsion angle H–C–N–C(=O), is similar in either foldamer of the triad, as well as in dyads, and is described as synperiplanar, with the torsion angle in the range 0 to −10°. This corresponds to the previously established minimum-energy structures of imides attached to a cyclohexane ring.[27]

The conclusion emerging from the computational study of isolated imide triads is quite simple: there is little energy difference between the corresponding *C* and *S* foldamers of the triads and it is in favor of the latter, except triads **1c** and **2c**. The significant differences in the magnitudes of the dipole moments of *C* and *S* foldamers of the triads do not seem to contribute significantly to destabilization of the *C* foldamers. In fact, dipole–dipole interactions appear to account fully for any energy difference between *C* and *S* foldamers. Therefore the conformationally bistable triads appear to be good candidates for studying the effect of the solvent on the mode of their folding.

2.3. ^{1}H NMR studies

Since the computational studies for isolated triad molecules do not reveal any significant bias toward either *C* or *S* foldamer there remains an intriguing question whether in solution one can observe a shift of the equilibrium between the populations of triad foldamers. To answer this question, we used the ^{1}H NMR spectra of triads in which the diimide proton signals show anisochrony, i.e., separate signals due to the diimide protons in each foldamer will appear in the spectra (Table 2).

In $CDCl_3$ solution, these signals appear conveniently in the 8.1–8.7 ppm spectral window. In the case of **2b** the 1,8-naphthalimide and 1,4,5,8-naphthalenedicarboximide signals overlap. Complete assignment of the signals in the aromatic portion of the spectrum was possible with the use of ^{1}H–^{1}H correlation NMR spectra. The two singlets (*S*) and doublets (*C*) of the diimide fragment, due to the two foldamers, were found at 8.36, 8.59 and 8.45, 8.53 ppm, respectively (Fig. 3).

Other ^{1}H NMR signals of the triads are not resolved at room temperature. This applies to the CH(N) signals, which appear in the range 5.0–5.9 ppm. Their position is dependent on the size of the imide ring and can be readily calculated using simple additivity of the shielding effect.[25] Thus in the case of triads **1a** and **1c** with two five-membered imide rings the CH(N) signals appear at ca. 5.0 ppm, whereas two six-membered imide rings (**2b**) shift the signal to ca. 6.4 ppm. Mixed type imides (**1b**, **2a**, **2c**) are characterized by two CH(N) signals at ca. 5.5 and 5.9 ppm (see Supplementary data).

The imide triads are poorly soluble in certain solvents (e.g., acetone, methanol), nevertheless we were able to obtain the NMR spectra in deuterated chloroform, benzene, hexafluorobenzene, and dimethyl sulfoxide (Table 3).

Table 2. Diastereotopic diimide proton signals in triads[28]

Diimide	Foldamer *C*	Foldamer *S*
1,2,4,5-Benzenedicarboxydiimide	One singlet	Two singlets
1,4,5,8-Naphthalenedicarboxydiimide	Two doublets	Two singlets

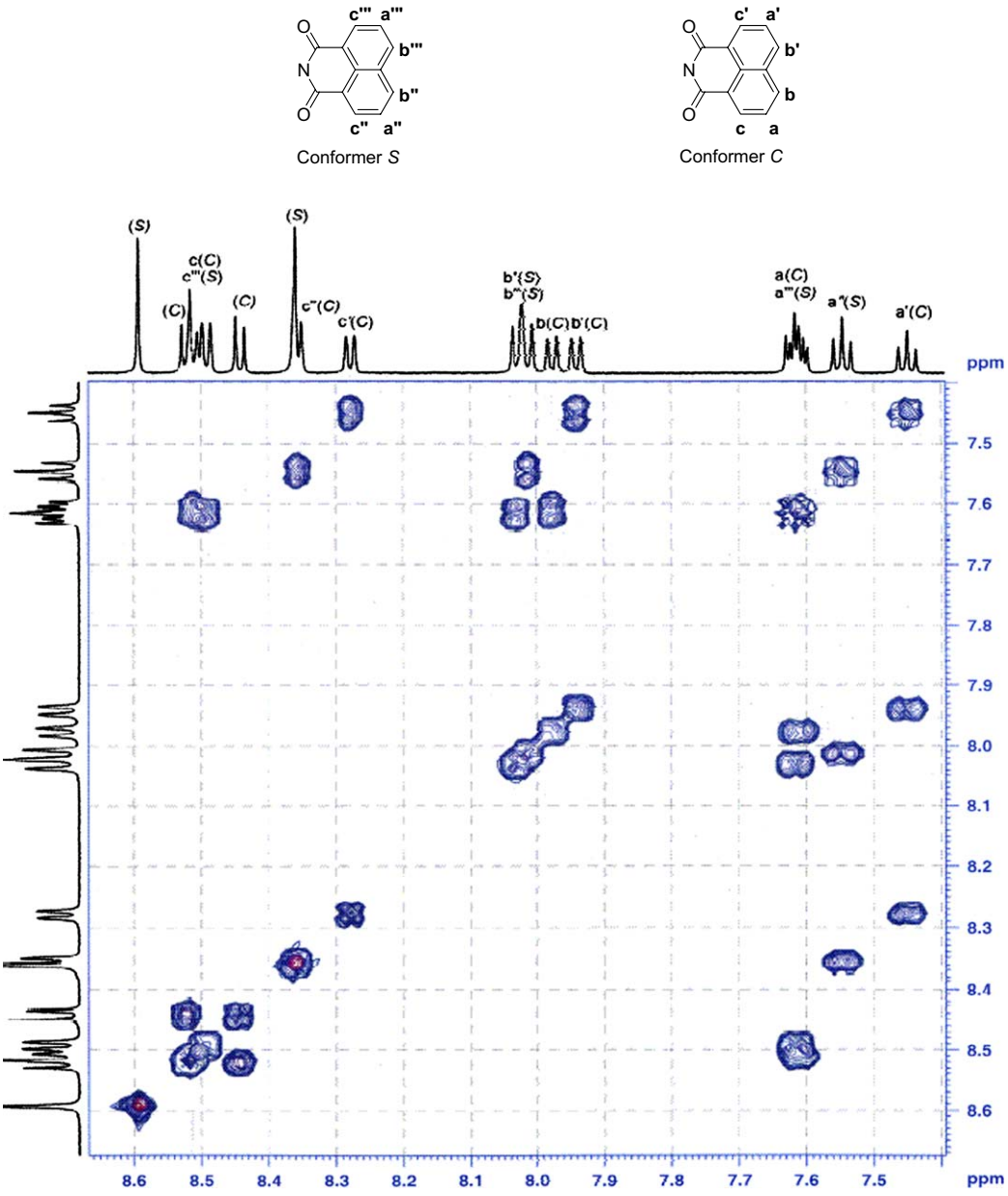

Figure 3. Aromatic protons region of ^{1}H–^{1}H correlation NMR spectrum of triad **2b**.

Another factor, limiting the analysis of the spectra, is a slow exchange of the diimide signals of pyromellitdiimides in **1a**–**1c** at room temperature, leading to broad, structureless signals. However, on lowering the temperature separate signals due to *C* and *S* foldamers could be obtained. Inspection of the data of Table 3 disclosed the preference for *C* foldamer in $CDCl_3$ solution. This preference increases upon lowering the temperature, up to the ratio *C*:*S*=67:33 for **1b** at 223 K. The only exception is triad **2b** for which a small preference for the *S* foldamer (*C*:*S*=45:55) was observed at 293 K. This could be due to the bulkiness of the naphthalene-based imide components of **2b**, destabilizing the *C* conformer.

Table 3. Ratio of *C*:*S* atropisomers of imide triads **1a**–**1c**, **2a**–**2c** in various solvents[a]

Triad	$CDCl_3$ (293 K)	$CDCl_3$, (273 K)	$CDCl_3$ (223 K)	C_6D_6 (293 K)	C_6F_6 (293 K)	$(CD_3)_2SO$ (293 K)
1a	[b]	54:46	60:40	[b]	[b]	[b]
1b	[b]	60:40	67:33	[b]	[b]	[b]
1c	[b]	50:50	56:44	[b]	[b]	[b]
2a	53:47	55:45	56:44	25:75	51:49	51:49
2b	45:55	46:54	47:53[c]	17:83	38:62	37:63
2c	52:48	54:46	55:45	[d]	[d]	58:42

[a] From integration of diimide ^{1}H NMR signals.
[b] Unresolved diimide ^{1}H NMR signals.
[c] At 253 K.
[d] Low solubility.

2.4. Circular dichroism study

Imide triads **1a**–**1c**, **2a**–**2c** are chiral trichromophoric systems whose CD spectra result primarily from exciton coupling of the allowed electronic transitions of component chromophores. Thus, the CD of a trichromophoric system can be treated as a sum of Cotton effects due to exciton coupling of the electronic transitions in each of the three chromophoric pairs. Therefore, the CD spectrum of a triad of

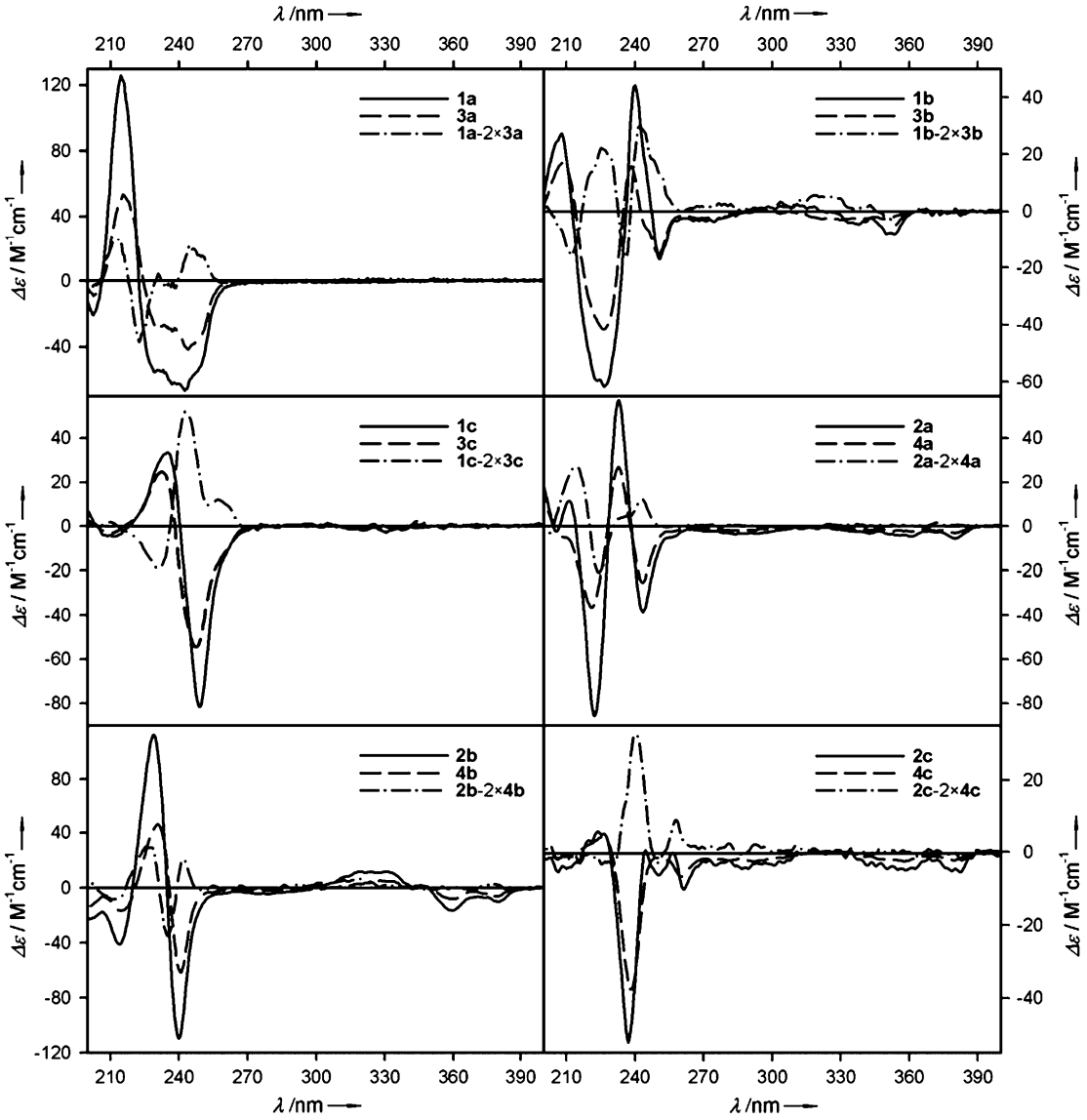

Figure 4. CD spectra of triads (——), the corresponding dyads (– – –) and the differential CD spectra: triad−2×dyad (· – · –), in acetonitrile solution.

the A–B–A type (**1a**–**1c**, **2a**–**2c**) can be considered as a sum of the two CD spectra of the corresponding dyads A–B (**3a**–**3c**, **4a**–**4c**) and the CD contribution due to exciton coupling of the two outer chromophores (A/A), Eq. 1.

$$\mathrm{CD(A-B-A)} \approx 2 \times \mathrm{CD(A-B)} + \mathrm{CD(A/A)} \qquad (1)$$

The CD contribution due to A/A coupling should be sensitive to triad conformation and it should change sign and/or magnitude with the change of the triad conformation between the stable *C* and *S* foldamers. Thus, by subtracting the experimental double CD spectrum of a dyad from the experimental CD spectrum of a triad one should get the differential CD spectrum reflecting the contribution due to the dominant foldamer of the triad. This approximation was found to work well with the triad **1a** and dyad **3a**. The differential CD spectrum indicated a strong negative exciton Cotton effect due to the phthalimide 220 nm transition and hence it was concluded that the *C* foldamer of **1a** was the dominant one in acetonitrile solution.[23]

We extended this approach to the other imide triads and dyads. Figure 4 shows their CD spectra in acetonitrile solution, as well as the corresponding differential CD spectra according to Eq. 1.

In addition, the validity of this experimental approach was checked (see Supplementary data) by comparison of the UV spectra of chromophores A of the triads A–B–A with the differential UV spectra obtained according to Eq. 2:

$$\mathrm{UV(A-B-A)} - \mathrm{UV(A-B)} \approx \mathrm{UV(A)} \qquad (2)$$

Within the exciton coupling approach, satisfactory results of comparison of the UV spectra were obtained.

In order to get a better understanding of the relation between the CD spectra and conformation of the imide triads we carried out computational simulation of the CD spectra within the semiempirical ZINDO/S method. The CD and UV spectra were calculated for the previously computed

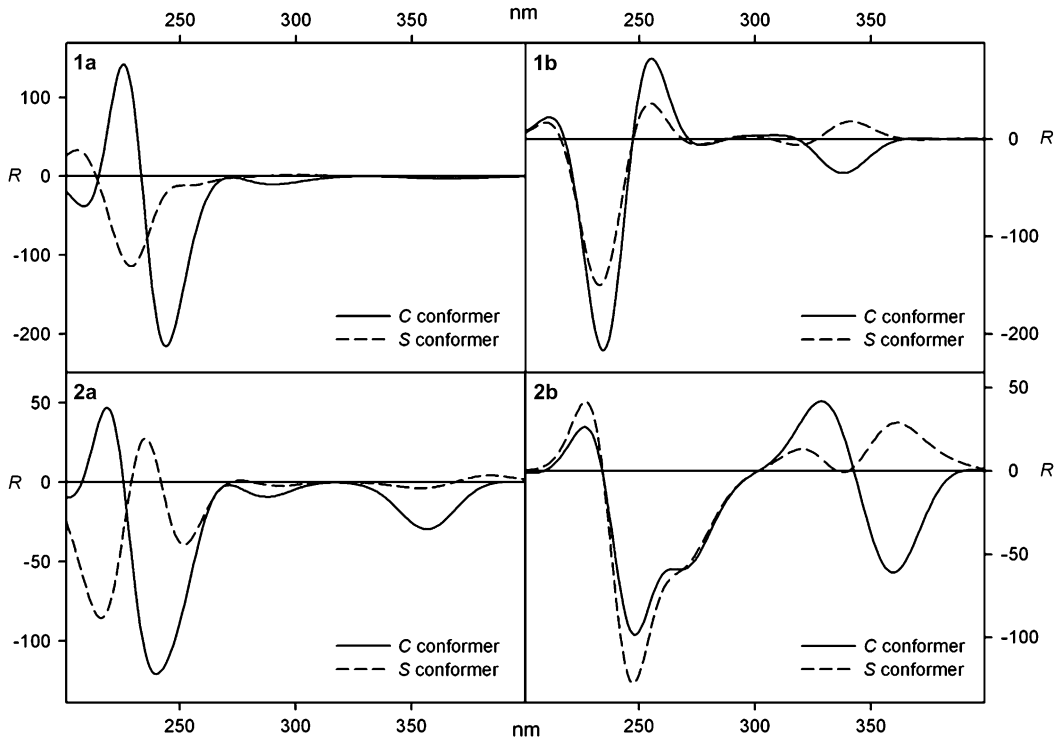

Figure 5. Calculated by ZINDO/S method CD spectra of C and S foldamers of triads **1a**, **1b**, **2a** and **2b**.

lowest-energy conformers of triads **1a**, **1b**, **2a**, **2b**. It was found that each CD and UV contour band of the calculated spectra is composed of several transitions of varying intensity (see Supplementary data). The shapes of the computed CD spectra of the *C* and *S* foldamers of triads **1a** and **2a** are different; in fact for the diagnostic 210–240 nm electronic transitions region of the phthalimide (PHT) chromophore system a strong negative exciton Cotton effect is obtained for the *C* foldamer, whereas a moderate, opposite-sign exciton Cotton effect is calculated for the *S* foldamer (Fig. 5).

This can be predicted on the basis of consideration of the relative orientation of the electronic dipole transition moments for the long axis polarized transitions of the PHT chromophores in **1a** and **2a**. Note that the computations are carried out for the lowest-energy foldamers of the triads, whereas in real molecules the conformers due to the rotation of the imide chromophores about the C–N axis will contribute significantly to the experimental CD spectrum. This occurs because the Cotton effects due to coupling of the electronic transitions polarized in the direction of the C–N bond axes will be independent of the imide chromophore rotation whereas those due to transitions polarized perpendicularly to the C–N bond axes will be averaged by rotation (weak contribution to the CD spectrum). The latter case refers to the transitions located at 240 nm in PHT, 248 nm in PYR, 231 nm in NDC and 239 nm in NTC chromophores (Fig. 6).

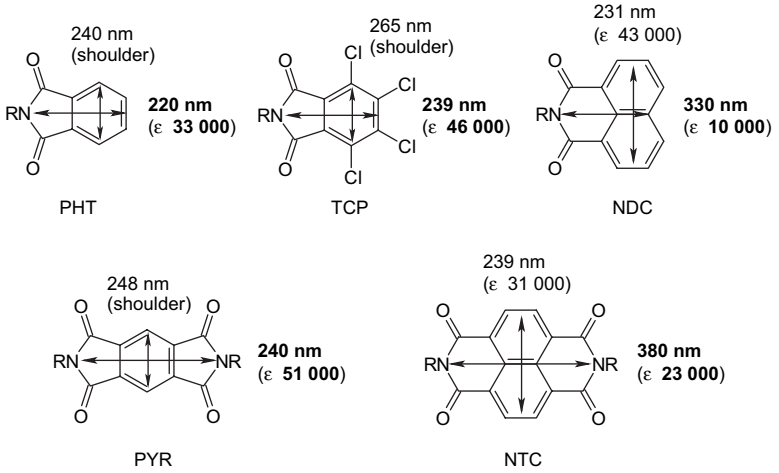

Figure 6. Most intense in-plane polarized π–π* transitions of aromatic mono- and diimides in the region 380–220 nm (data from Refs. 26, 27). The data for the diagnostic transitions, polarized in the direction of the R–N bond, are shown in bold.

For this reason, the calculated CD spectra of either foldamer of **1a** and **2a** in Figure 5 show significant (negative) CD contributions around 250 nm (in the case of foldamer *S* of **1a** a canceling effect of the positive long-wavelength part of the exciton Cotton effect due to the long axis polarized transition with the negative Cotton effect of the perpendicularly polarized transition was observed).

A less clear situation was found in the case of the CD spectra of triads **1b** and **2b**, having 1,8-naphthalimide chromophores. Here (Fig. 5) the calculated CD spectra of the *C* and *S* foldamers differ only in their magnitudes in the range of the most intense transitions (210–250 nm). However, opposite-sign Cotton effects are clearly seen in the region 330–370 nm, corresponding to the naphthalimide transition polarized along the imide rotation axis (Fig. 6). Thus, for the *C* foldamers of **1b** and **2b** a negative and for the *S* foldamers a positive long-wavelength Cotton effect is obtained, as anticipated for the transitions not affected by rotation of the chromophore.

These computational results demonstrate that reliable differentiation of the *C* and *S* foldamers of imide triads can only be achieved by the analysis of Cotton effects due to electronic transitions polarized in the direction of the imide rotational axis, as the rotatory strength in this case is independent of rotation. In the case of electronic transitions polarized perpendicularly to the axis of rotation the Cotton effects are evidently highly sensitive to the imide rotamer population (dynamic model) and the calculation of the rotational strength for a single 'frozen' rotamer of the triad (static model) does not reflect the situation found in real molecules.

Returning to the experimental CD spectra of the triads, we note that despite their complexity, useful information could be obtained from the analysis of Cotton effects resulting from coupling of the transitions polarized in the direction of imide rotational axis. As expected, both triad **1a** and dyad **3a** display a negative exciton Cotton effect centered at 215–220 nm, due to coupling of the long axis polarized transitions of PHT and PYR (Fig. 4). The differential CD spectrum also shows a negative exciton Cotton effect ($\Delta\varepsilon$ −37.0 at 223 nm, +25.6 at 213 nm). This can be interpreted as the effect of the dominant *C* foldamer of triad **1a**. Such a conclusion should be taken with caution since the CD contributions of each *C* and *S* foldamer are of opposite sign but not of the same magnitudes.

The CD spectrum of triad **2a** displays several Cotton effects in the region below 300 nm. In contrast, the differential CD spectrum of **2a**−2×**4a** (Fig. 4) is quite simple, resembling that of **1a**−2×**3a**. Thus, besides a positive CD maximum at 245 nm a negative exciton Cotton effect is found in the region of PHT absorption ($\Delta\varepsilon$ −36.2 at 223 nm, +25.6 at 214 nm). As in the case of **1a**, this can be interpreted as a characteristic spectral signature of the *C* foldamer of **2a**.

A similar analysis can be carried out for triad **1c** and dyad **3c**, as well as for **2c** and **4c**, where the principal role in exciton coupling can be ascribed to the long axis polarized transitions of the TCP chromophores. Whereas **1c** and **3c** as well as **2c** and **4c** show the expected negative exciton Cotton effect centered at ca. 240 nm, the differential CD spectra feature positive exciton Cotton effects ($\Delta\varepsilon$ +51.9 at 243 nm, −19.3 at 231 nm for **1c** and +32.7 at 241 nm, −3.3 at 226 nm for **2c**). This is a strong indication of the dominant *S* foldamer of triads **1c** and **2c**, contrasting with the preference of *C* foldamer in non-chlorinated analogs **1a** and **2a**, in acetonitrile solution.

Rather complex experimental CD spectra characterize the triads and dyads incorporating the naphthalene-based imide chromophores (NDC, NTC). For example, at least four Cotton effects can be seen in the CD spectra of imide triad **1b** and dyad **3b** in the region 210–260 nm. We therefore use for the conformational analysis the long-wavelength Cotton effects due to the coupling of the NDC chromophore transitions. Since the experimental long-wavelength Cotton effects of **1b** as well as **2b** are negative we conclude that in both cases the more stable foldamer in acetonitrile solution is *C*.

In short, the analysis of the CD spectra of imide triads is highly complicated and hindered by the inadequacy of currently available computational protocols to provide exact results including the effect of rotation of the chromophores. A comparison of experimental and calculated CD spectra of triads and dyads shows that foldamer *C* is the dominant one for all non-chlorinated imide triads **1a**, **1b**, **2a** and **2b** whereas foldamer *S* is the preferred one in the case of **1c** and **2c** in acetonitrile solution.

2.5. Crystal structure of triad 2a inclusion compound

We were able to obtain crystals suitable for X-ray diffraction analysis for triads **1a** and **2a**. X-ray data for **1a** have already been published[23] while those for **2a** are the subject of this presentation. Both compounds crystallize with planar aromatic molecules as guests, with the host to guest ratio 1:2, and both adopt the extended *S* conformation. Although the two crystal structures differ in the mode the host and guest molecules pack in the crystal, one can define two basic supramolecular motifs that are common for both crystal structures. One of these motifs, which might be described as tri-aromatic stack, consists of a host diimide molecule surrounded on both sides by planar aromatic solvent molecules (pyridine in **1a** and benzene in **2a**). The three molecules (i.e., two guest and one host) are engaged in face-to-face stacking interactions. This is illustrated for **2a** in Figure 7a,b.

The distance from the center of the diimide moiety to the centers of the two benzene rings amounts to 3.749 and 3.835 Å and the rings are parallel to within 5°. The other supramolecular motif that is common for the crystal structures of **1a** and **2a** involves the host molecules that are engaged in C–H(cyclohexane)$\cdots\pi_c$(PHT) pair-wise interactions [π_c(PHT) describes the center of the benzene ring that is a part of the phthalimide moiety]. These interactions are responsible for joining the host molecules into infinite chains. In the crystal of **2a**, the chains run parallel to [101] direction and the H$\cdots\pi_c$(PHT) distances and C–H$\cdots\pi_c$(PHT) angles amount to 2.95 and 2.92 Å and 158 and 156°, respectively. The host–host interactions in the crystal structure of **2a** are further supplemented by the C–H(cyclohexane)$\cdots$O=C hydrogen bonds (2.47 Å and 140° for H$\cdots$O distance and C–H$\cdots$O angle, respectively) by which the [101] molecular chains are extended into the (010) layers. The benzene guest

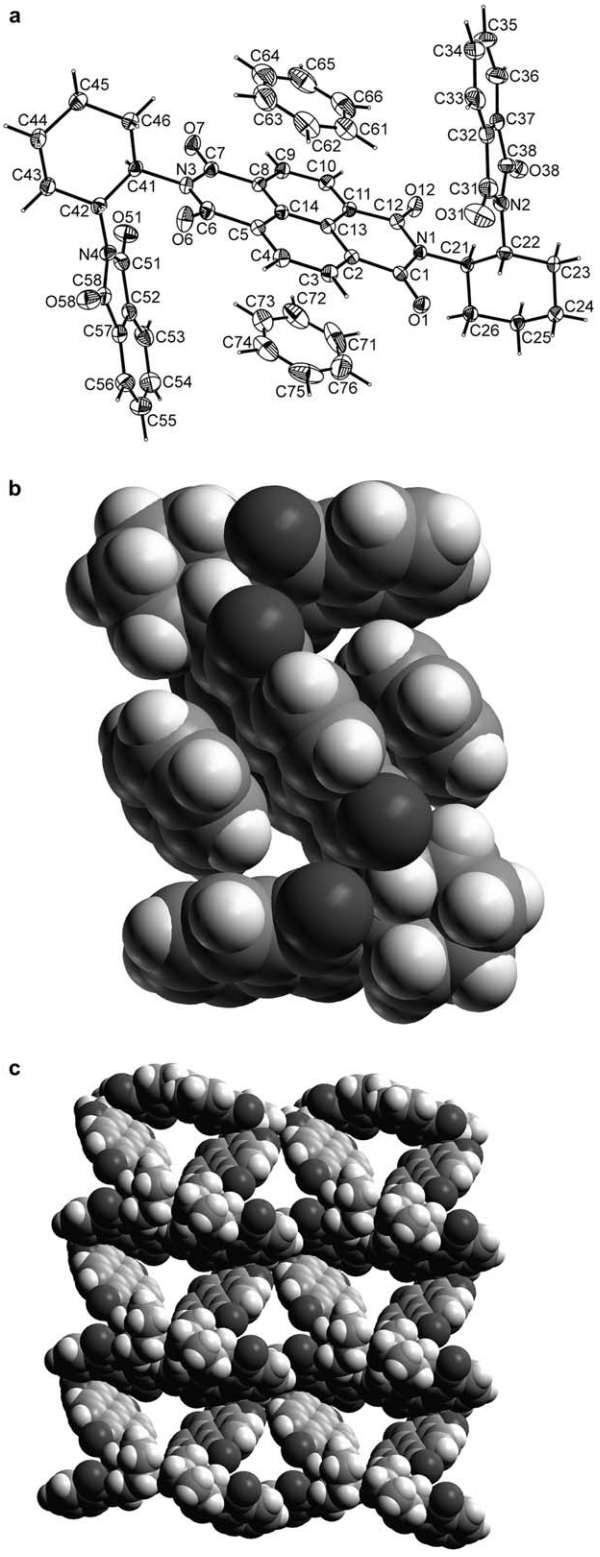

Figure 7. (a) Perspective view of the content of the independent part of the unit cell. Thermal ellipsoids are drawn at 40% probability level and give a graphical representation of atomic displacements at 150 K; (b) the basic supramolecular motif—the imide triad **2a** and the two benzene molecules—glued together by face-to-face stacking interactions; (c) view along the *c*-direction illustrating the porosity of the crystal structure. Host molecules are represented as van der Waals spheres, guest molecules are omitted.

molecules in the crystal of **2a** are arranged in channels running along the *c*-direction (Fig. 7c). There are two such channels per unit cell, related to each other by the two-fold screw axis. The guest accessible volume per unit cell amounts to 594 Å^3, which means that approximately 27% of the crystal volume is available for including guests.[29] A term 'porosity' has been used in the literature when referring to the latter value. Unlike the pyridine guest molecules in **1a**, which engage in stacking interactions between themselves, the benzene guest molecules in **2a** seem to be involved solely in the face-to-face stacking interactions with the host.

The inherently preferred synperiplanar conformation of the cyclic imide moiety with respect to the attached cyclohexane, established by the theoretical calculations (vide supra), and described by the magnitude of the torsion angle H–C–N–C(=O), is also observed in the presented crystal structure of **2a**. However, as the molecule does not utilize its C_2 symmetry in the crystal lattice, the torsion angle values differ significantly at the two ends of the molecule: the H22–C22–N2–C31 and H21–C21–N1–C12 torsion angles amount to −5 and 5°, respectively, while the H41–C41–N3–C7 and H42–C42–N4–C58 angles adopt the values of 25 and 21°, respectively. A CSD search (2005 release)[30] carried out for cyclic imides attached to cyclohexane (17 observations) revealed that in the solid state the magnitudes of the H–C–N–C(=O) torsion angles vary from 0 to 23°. Nonetheless, the fact that imide group prefers the synperiplanar orientation for one of its carbonyl bonds with respect to the cyclohexane C–H bond must be due to additional attractive interactions. We see this in 1,3-(C=O)/(H–C) antiparallel dipole–dipole interactions and/or in intramolecular C–H···O=C hydrogen bonds that close both 5- and 6-membered rings.

3. Conclusions

Imide triads, derived from *trans*-1,2-diaminocyclohexane and aromatic anhydrides, can exist in the dynamic equilibrium of two diastereomeric folded structures of *C* and *S* shape. This equilibrium reflects the process of helix *M*–helix *P* transition for each triad. Whereas the calculated energy difference between the foldamers is low (<0.1 kcal mol^{-1}) the equilibrium in solution can be significantly altered. For example, the *C*:*S* ratio is 2:1 for triad **1b** in $CDCl_3$ solution at 223 K, whereas the ratio 1:5 was measured for **2b** in C_6D_6 solution at 293 K. The effect of aromatic solvent molecules stabilizing *S* foldamer of the triad can be adequately explained by a truncated model emphasizing the donor–acceptor interactions (Fig. 8).

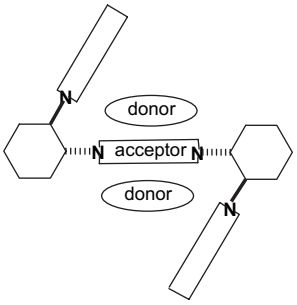

Figure 8. A model for the donor–acceptor interaction between *S* foldamer of the imide triad and donor solvent molecules.

This sandwich-type model is based on the X-ray determined structures of **2a**×2 benzene (present work) and **1a**×2 pyridine clathrates.[23] Both ^{1}H NMR and CD spectroscopy are potentially useful for studying the foldamer population in solution, with the limitations intrinsic for each method. For the NMR method, the rate of exchange between the folded *C* and *S* structures is of paramount importance and the signal separation could be observed for aromatic protons of the 1,2,4,5-benzenetetracarboxydiimide core in triads **1a**–**1c** at lowered temperatures only. The helical *C* and *S* structures feature signature CD spectra, according to ZINDO/S calculations. However, the analysis of the CD spectra is of only limited use because of the complex nature of the experimental CD spectra and inadequacy of the static computational models, not including the rotation of the imide chromophores in real molecules, to reproduce correctly the chiroptical properties of the foldamers. Nevertheless, by carefully choosing the CD spectral window, corresponding to electronic transitions polarized in the direction of the axis of rotation, the estimation of the preferred foldamer in the equilibrium was possible. Such an analysis indicated the preference of *S* foldamer of the triads **1c** and **2c**, containing the tetrachlorophthalimide fragments, in acetonitrile solution.

4. Experimental

4.1. General

NMR spectra were recorded on Varian XL300 or Bruker Avance DRX 600 instruments and are reported in parts per million with respect to TMS as a reference. CD and UV spectra were measured on a JASCO 810 spectropolarimeter in acetonitrile solution. MS were recorded with a AMD 604 Intectra or AMD 402 Intectra spectrometers. FTIR spectra were taken in KBr pellets on a Bruker IFS 113v spectrometer. Elemental analyses were performed with a Perkin–Elmer 2400 CHNS/O analyzer. Melting points are uncorrected. TLC plates (silica gel on alumina foil) were developed with hexane–ethyl acetate (3:1); R_f values were ca. 0.6 for triads **1a**–**1c**, **2a**–**2c** and 0.85 for dyads **3a**–**3c**, **4a**–**4c**.

4.2. Preparation of triads 1a–1c, 2a–2c

4.2.1. Method A. A mixture of appropriate DACH derivative **5a**, **5b** or **5c**[25] (2 mmol) and 1,4,5,8-naphthalenetetracarboxylic dianhydride (268 mg, 1 mmol) or pyromellitic dianhydride (218 mg, 1 mmol) in DMF (10 ml) was stirred at 90 °C until homogeneous solution was obtained. After that, stirring at 120–130 °C was continued for 6 h. The solution was evaporated in vacuo. The product was purified by column chromatography on silica gel using mixtures of CH_2Cl_2 and AcOEt as eluent, followed by crystallization.

4.2.1.1. Triad 1a. Yield 18%, mp 342–344 °C; ^{1}H NMR δ 1.50–1.66 (m, 6H, $CH_{cycl.}$), 1.89–1.91 (m, 6H, $CH_{cycl.}$), 2.41–2.44 (m, 4H, $CH_{cycl.}$), 4.97 (m, 4H, CH–N), 8.2 (br s, 10H, CH_{Ar}); ^{13}C NMR δ 24.83, 24.86, 50.77, 53.40, 118.4, 123.31, 131.01, 133.98, 136.84, 136.05, 136.84, 165.76, 167.97; CD (acetonitrile) $\Delta\varepsilon$ (nm) −66.9 (243), +125.6 (215), −20.7 (202); UV (acetonitrile) ε (nm) 4800 (297), 65,900 (235), 103,900 (220); IR ν (cm^{-1}) 3080, 3066, 2937, 2859, 1772, 1720, 1380, 1110, 872, 730, 631; FABHRMS: calcd for $C_{38}H_{31}O_8N_4$ (M+1): 671.2142, found: 671.2142.

4.2.1.2. Triad 1b. Yield 13%, mp>360 °C; ^{1}H NMR δ 1.48–1.67 (m, 5H, $CH_{cycl.}$), 1.8–2.0 (m, 7H, $CH_{cycl.}$), 2.34–2.7 (m, 4H, $CH_{cycl.}$), 5.49 (dt, *J*=3.3, 11.5 Hz, 2H, CH–N), 5.81 (dt, *J*=3.82, 11.5 Hz, 2H, CH–N), 7.15–7.62 (m, 2H, CH_{Ar}), 7.69 (t, *J*=7.7 Hz, 3H, CH_{Ar}), 8.10 (t, *J*=7.7 Hz, 5H, CH_{Ar}), 8.35 (br s, 2H, CH_{Ar}), 8.54 (d, *J*=7.1 Hz, 2H, CH_{Ar}); ^{13}C NMR δ 25.03, 25.26, 28.51, 29.46, 29.67, 50.88, 53.23, 118.20, 121.97, 122.63, 126.77, 127.02, 128.05, 128.30, 131.21, 131.29, 131.63, 133.61, 133.75, 135.98, 136.68, 164.26, 164.45, 165.94; CD (acetonitrile) $\Delta\varepsilon$ (nm) −7.9 (355), −4.5 (338), −17.0 (251), +44.1 (240), −61.7 (226), −59.5 (224), +27.3 (208); UV (acetonitrile) ε (nm) 20,300 (343), 22,700 (333), 19,800 (324), 17,600 (251), 106,100 (233), 45,400 (208); IR ν (cm^{-1}) 3096, 2932, 2868, 1770, 1714, 1664, 1586, 1356, 1237, 1108, 780; Anal. Calcd for $C_{46}H_{34}N_4O_8$: C, 71.69; H, 4.45; N, 7.27. Found: C, 71.58; H, 4.40; N, 7.26.

4.2.1.3. Triad 1c. Yield 12%, mp>360 °C; ^{1}H NMR δ 1.17–1.80 (m, 6H, $CH_{cycl.}$), 1.90–1.93 (m, 6H, $CH_{cycl.}$), 2.17–2.70 (m, 4H, $CH_{cycl.}$), 4.96 (m, 4H, CH–N), 8.15 (br s, 2H, CH_{Ar}); ^{13}C NMR δ 23.80, 24.74, 24.78, 28.81, 28.88, 51.29, 51.75, 118.75, 126.63, 127.14, 128.31, 129.74, 136.29, 140.36, 163, 14, 165.72; CD (acetonitrile) $\Delta\varepsilon$ (nm) −81.5 (249), +33.4 (235), −4.6 (212); UV (acetonitrile) ε (nm) 177,400 (238): IR ν (cm^{-1}) 3478, 2936, 2865, 1770, 1728, 1345, 1111, 825, 734; Anal. Calcd for $C_{38}H_{22}N_4O_8Cl_8$: C, 48.24; H, 2.34; N, 5.92. Found: C, 48.20; H, 2.53; N, 5.88.

4.2.1.4. Triad 2a. Yield 16%, mp>360 °C; ^{1}H NMR δ 1.18–1.60 (m, 4H, $CH_{cycl.}$), 1.90–2.1 (m, 8H, $CH_{cycl.}$), 2.47–2.67 (m, 4H, $CH_{cycl.}$), 5.42 (dt, *J*=4.6, 11.8 Hz, 2H, CH–N), 5.87 (tt, *J*=3.1, 8.1 Hz, 2H, CH–N), 7.19–7.64 (br s, 8H, CH_{Ar}), 8.46 (s, 1H), 8.53 (d, *J*=7.4 Hz, 1H, CH_{Ar}), 8.61 (d, *J*=7.4 Hz, 1H, CH_{Ar}), 8.70 (s, 1H, CH_{Ar}); ^{13}C NMR δ 25.21, 25.25, 25.43, 25.46, 28.66, 29.60, 29.73, 29.78, 50.33, 123.01, 123.13, 125.81, 125.89, 126.76, 126.85, 130.60, 130.88, 130.99, 131.28, 131.48, 133.58, 133.66, 162.73, 162.98, 163.03, 167.91, 168.03; CD (acetonitrile) $\Delta\varepsilon$ (nm) −5.3 (381), −3.2 (343), −3.6 (284), −38.7 (244), +57.0 (233), −85.6 (223), +11.4 (211), −2.1 (206), +20 (200); UV (acetonitrile) ε (nm) 26,800 (381), 21,900 (360), 7000 (300), 4500 (233), 78,600 (221); IR ν (cm^{-1}) 2956, 2875, 1775, 1710, 1680, 1663, 1380, 1330, 1245, 1110, 887, 725; FABMS: *m*/*z* 721.3 [M+H]; Anal. Calcd for $C_{42}H_{32}N_4O_8$: C, 69.99; H, 4.47; N, 7.77. Found: C, 70.18; H, 4.46; N, 7.79.

4.2.1.5. Triad 2b. Yield 13%, mp>360 °C; ^{1}H NMR δ 1.25–1.69 (m, 4H, $CH_{cycl.}$), 2.05–2.18 (m, 8H, $CH_{cycl.}$), 2.63–2.67 (m, 4H, $CH_{cycl.}$), 6.30 (m, 4H, CH–N), 7.46 (t, *J*=7.7 Hz, 1H, CH_{Ar}), 7.55 (t, *J*=7.7 Hz, 1H, CH_{Ar}), 7.63 (t, *J*=7.4 Hz, 2H, CH_{Ar}), 7.94 (d, *J*=9.3 Hz, 1H, CH_{Ar}), 8.03 (d, *J*=6.2 Hz, 2H, CH_{Ar}), 8.05 (d, *J*=6.2 Hz, 1H, CH_{Ar}), 8.27 (d, *J*=6.3 Hz, 1H, CH_{Ar}), 8.36 (d, *J*=6.2 Hz, 2H, CH_{Ar}), 8.37 (s, 1H, CH_{Ar}), 8.48 (d, *J*=7.7 Hz, 1H, CH_{Ar}), 8.49 (d, *J*=6.2 Hz, 1H, CH_{Ar}), 8.52 (d, *J*=6.1 Hz, 1H, CH_{Ar}), 8.59 (s, 1H, CH_{Ar}); ^{13}C NMR δ 25.65, 29.34,

29.413, 29.78, 53.06, 53.19, 53.81, 122.26, 122.33, 123.13, 123.19, 125.90, 126.24, 126.44, 126.61, 126.70, 126.78, 127.97, 130.39, 130.57, 130.74, 130.87, 130.96, 131.12, 131.17, 131.23, 131.34, 133.11, 133.19, 133.31; CD (acetonitrile) $\Delta\varepsilon$ (nm) −9.9 (381), −16.4 (359), +1.80 (346), +11.8 (331), −4.8 (279), −111.2 (240), −42.5 (214); UV (acetonitrile) ε (nm) 24,200 (380), 32,900 (341), 19,800 (324), 100,900 (231); IR ν (cm^{-1}) 2926, 2853, 1704, 1672, 1587, 1342, 1237, 1106, 780; FABMS: *m/z* 821.3 [M+H]; Anal. Calcd for $C_{50}H_{36}N_4O_8$: C, 73.16; H, 4.42; N, 6.83. Found: C, 72.58; H, 4.40; N, 6.86.

4.2.1.6. Triad 2c. Yield 14%, mp>360 °C; ^{1}H NMR δ 1.49–1.65 (m, 6H, $CH_{cycl.}$), 1.85–2.0 (m, 6H, $CH_{cycl.}$), 2.4–2.68 (m, 4H, $CH_{cycl.}$), 5.46 (dt, *J*=3.8, 11.5 Hz, 2H, CH–N), 5.83 (dt, *J*=3.3, 11.3 Hz, 2H, CH–N), 8.56 (s, 1H, CH_{Ar}), 8.61 (d, *J*=7.1 Hz, 1H, CH_{Ar}), 8.67 (d, *J*=7.24 Hz, 1H, CH_{Ar}), 8.73 (s, 1H, CH_{Ar}); ^{13}C NMR δ 25.37, 28.69, 29.12, 29.45, 51.21, 53.79, 54.45, 125.58, 126.36, 126.47, 126.91, 127.06, 129.43, 130.50, 130.78, 130.99, 131.33, 139.85, 162.78, 162.93, 163.11; UV (acetonitrile) ε (nm) 23,200 (380), 19,100 (360), 14,300 (340), 5200 (271), 85,400 (237); CD (acetonitrile) $\Delta\varepsilon$ (nm) −5.52 (383), −4.9 (359), −10.2 (261), −52.2 (237), +5.5 (224); IR ν (cm^{-1}) 2931, 2856, 1776, 1722, 1666, 1579, 1452, 1345, 1190, 1104; Anal. Calcd for $C_{42}H_{24}N_4O_8Cl_8$: C, 50.64; H, 2.43; N, 5.62. Found: C, 50.82; H, 2.41; N, 5.58.

4.2.2. Method B. A mixture of **5a** (488 mg, 2 mmol) or **5c** (764 mg, 2 mmol) and pyromellitic anhydride (218 mg, 1 mmol) was stirred under reflux in glacial acetic acid (5 ml) for 6 h. The solution was evaporated in vacuo. The product was purified as in method A. Yield **1a**: 44%, **1c**: 48%.

4.3. Preparation of dyads 3a–3c, 4a–4c

Monoanhydride of *N*-cyclohexyl-1,4,5,8-naphthalenetetracarboxymonoimide (349 mg, 1 mmol) or monoanhydride of *N*-cyclohexyl-1,2,4,5-benzenetetracarboxymonoimide (299 mg, 1 mmol)[26] and appropriate DACH derivative **5a**, **5b** or **5c**[25] (1 mmol) in DMF (10 ml) was heated with stirring at 120–130 °C for 5 h. The solution was evaporated in vacuo. The product was purified by column chromatography on silica gel, using hexane–CH_2Cl_2 and CH_2Cl_2 as eluents, followed by crystallization.

4.3.1. Dyad 3a. Yield 42%, mp 233–236 °C; ^{1}H NMR δ 1.28–1.30 (m, 3H, $CH_{cycl.}$), 1.53–1.57 (m, 3H, $CH_{cycl.}$), 1.67–1.70 (m, 3H, $CH_{cycl.}$), 1.90–2.2 (m, 6H, $CH_{cycl.}$), 2.13–2.15 (m, 2H, $CH_{cycl.}$), 2.42–2.45 (m, 1H, $CH_{cycl.}$), 4.11 (m, 1H, CH–N), 5.01 (m, 2H, CH–N), 8.2 (br s, 6H, CH_{Ar}); CD (acetonitrile) $\Delta\varepsilon$ (nm) −41.7 (244), +53.4 (216), −8.5 (203); UV (acetonitrile) ε (nm) 3200 (304), 59,900 (237), 64,700 (220); FABHRMS: calcd for $C_{30}H_{28}O_6N_3$ (M+1): 526.1978, found: 526.1956.

4.3.2. Dyad 3b. Yield 38%, mp>360 °C; ^{1}H NMR δ 1.18–1.39 (m, 4H, $CH_{cycl.}$), 1.61–1.67 (m, 6H, $CH_{cycl.}$), 1.81–2.13 (m, 6H, $CH_{cycl.}$), 2.15–2.72 (m, 2H, $CH_{cycl.}$), 4.07 (dt, *J*=3.3, 11.3 Hz, 1H, CH–N), 5.59 (dt, *J*=3.5, 11.6 Hz, 1H, CH–N), 5.89 (dt, *J*=3.8, 11.5 Hz, 1H, CH–N), 7.59 (t, *J*=7.4 Hz, 1H, CH_{Ar}), 7.75 (t, *J*=7.5 Hz, 1H, CH_{Ar}), 8.1 (br s, 2H, CH_{Ar}), 8.15 (t, *J*=7.4 Hz, 2H, CH_{Ar}), 8.43 (d, *J*=7.7 Hz, 1H, CH_{Ar}), 8.43 (d, *J*=7.7 Hz, 1H, CH_{Ar}); CD (acetonitrile) $\Delta\varepsilon$ (nm) −2.6 (332), −2.6 (276), −15.1 (251), +15.7 (239), −41.6 (227), +16.9 (209); UV (acetonitrile) ε (nm) 10,600 (342), 12,100 (333), 21,100 (251), 81,500 (234), 38,700 (214); Anal. Calcd for $C_{34}H_{29}N_3O_6$: C, 70.95; H, 4.99; N, 7.46. Found: C, 70.95; H, 5.08; N, 7.32.

4.3.3. Dyad 3c. Yield 58%, mp 162–165 °C; ^{1}H NMR δ 1.22–1.53 (m, 5H, $CH_{cycl.}$), 1.72–1.85 (m, 3H, $CH_{cycl.}$), 1.9–1.93 (m, 6H, $CH_{cycl.}$), 2.1–2.22 (m, 2H, $CH_{cycl.}$), 2.36–2.45 (m, 2H, $CH_{cycl.}$), 4.12 (tt, *J*=3.6, 11.7 Hz, 1H, CH–N), 4.39–5.01 (m, 2H, CH–N), 8.15 (br s, 2H, CH_{Ar}); CD (acetonitrile) $\Delta\varepsilon$ (nm) −54.5 (248), +24.5 (234), −3.3 (211); UV (acetonitrile) ε (nm) 102,700 (237). Elemental analysis: calcd for $C_{30}H_{23}N_3O_6Cl_4$: C, 54.32; H, 3.49; N, 6.33%; obtained: C, 54.26; H, 3.53; N, 6.30%.

4.3.4. Dyad 4a. Yield 32%, mp 165–170 °C; ^{1}H NMR δ 1.27–1.87 (m, 9H, $CH_{cycl.}$), 1.86–1.96 (m, 5H, $CH_{cycl.}$), 2.43–2.70 (m, 4H, $CH_{cycl.}$), 4.97 (dt, *J*=3.6, 12.1 Hz, 1H, CH–N), 5.46 (dt, *J*=3.6, 11.5 Hz, 1H, CH–N), 5.91 (dt, *J*=4.1, 11.5 Hz, 1H, CH–N), 7.28–7.61 (m, 4H, CH_{Ar}), 8.59 (s, 2H, CH_{Ar}), 8.68 (d, *J*=7.7 Hz, 1H, CH_{Ar}), 8.74 (d, *J*=7.7 Hz, 1H, CH_{Ar}); CD (acetonitrile) $\Delta\varepsilon$ (nm) −3.0 (380), −2.1 (371), −2.5 (362), −25.4 (243), +26.8 (233), −34.5 (223); UV (acetonitrile) ε (nm) 26,400 (380), 21,800 (360), 38,100 (235), 49,800 (221). EIHRMS: calcd for $C_{34}H_{29}O_6N_3$ (M): 575.2056, found: 575.2072.

4.3.5. Dyad 4b. Yield 42%, mp>360 °C; ^{1}H NMR δ 1.25–2.06 (m, 12H, $CH_{cycl.}$), 2.04–2.49 (m, 3H, $CH_{cycl.}$), 2.68–2.72 (m, 3H, $CH_{cycl.}$), 4.93 (tt, *J*=3.6, 12.3 Hz, 1H, CH–N), 6.32 (dt, *J*=4.1, 11.0 Hz, 1H, CH–N), 6.39 (dt, *J*=3.9, 11.0 Hz, 1H, CH–N), 7.56 (t, *J*=7.4 Hz, 1H, CH_{Ar}), 7.64 (t, *J*=7.4 Hz, 1H, CH_{Ar}), 8.05 (t, *J*=7.3 Hz, 2H, CH_{Ar}), 8.39 (d, *J*=7.1 Hz, 1H, CH_{Ar}), 8.46–8.55 (m, 1H, CH_{Ar}), 8.53 (s, 2H, CH_{Ar}), 8.61 (d, *J*=7.7 Hz, 1H, CH_{Ar}), 8.70 (d, *J*=7.7 Hz, 1H, CH_{Ar}); CD (acetonitrile) $\Delta\varepsilon$ (nm) −6.2 (380), −8.2 (360), +5.0 (332), −63.4 (240), +47.1 (230), −16.1 (216); UV (acetonitrile) ε (nm) 24,000 (379), 23,000 (341), 63,300 (232); Anal. Calcd for $C_{38}H_{30}N_3O_6$: C, 73.07; H, 4.84; N, 6.73. Found: C, 72.95; H, 4.82; N, 6.67.

4.3.6. Dyad 4c. Yield 48%, mp 177–180 °C; ^{1}H NMR δ 0.88–0.9 (m, 2H, $CH_{cycl.}$), 1.25–1.95 (m, 12H, $CH_{cycl.}$), 2.42–2.68 (m, 4H, $CH_{cycl.}$), 4.98 (dt, *J*=3.8, 8.5 Hz, 1H, CH–N), 5.50 (dt, *J*=4.0, 11.8 Hz, 1H, CH–N), 5.86 (dt, *J*=3.8, 11.5 Hz, 1H, CH–N), 8.63 (s, 2H, CH_{Ar}), 8.69 (d, *J*=7.6 Hz, 1H, CH_{Ar}), 8.74 (d, *J*=7.4 Hz, 1H, CH_{Ar}); CD (acetonitrile) $\Delta\varepsilon$ (nm) −2.3 (380), −6.8 (261), −37.7 (239), +4.0 (225); UV (acetonitrile) ε (nm) 21,900 (379), 10,900 (366), 17,600 (359), 11,700 (340), 64,900 (237); Anal. Calcd for $C_{34}H_{25}N_3O_6Cl_4$: C, 57.25; H, 3.53; N, 5.89. Found: C, 57.13; H, 3.54; N, 5.77.

5. X-ray structure determination of 2a

Triad **2a** crystallized from benzene as an inclusion compound with the formula $C_{42}H_{32}N_4 \cdot 2C_6H_6$, M_r=876.93, *T*=150 K. Crystal system: monoclinic. Space group: $P2_1$.

Unit cell dimensions: a=11.354(2), b=16.712(3), c=11.413(2) Å, β=90.50(3)°; V=2165.5(7) Å^3; Z=2; ρ_{cal}=1.345 Mg m^{-3}; Mo Kα (λ=0.71073, ω-scan); μ=0.091 mm^{-1}. Final R value 0.0560 for 3370 observed reflections [$I>2\sigma(I)$]. Crystal size: 0.3×0.4×0.3 mm^3. Data was collected with a KM4CCD kappa-geometry diffractometer[31] equipped with graphite monochromator. Theta range for data collection was 4.17–25.03° and the *hkl* ranges were −13/13, −19/9, −13/13, respectively. Of the 10,777 reflections collected, 3884 were unique (R_{int}=0.0510) and 3370 were considered as observed with $I>2\sigma(I)$. The intensity data were corrected for *Lp* effects. No absorption correction was applied.

Data reduction and analysis were carried out with the CrysAlisRED.[31] The structure was solved by direct methods using SHELXS-97,[32,33] and refined by the full matrix least-squares techniques with SHELXL-97.[34] Non-hydrogen atoms were refined anisotropically. The positions of all H atoms attached to carbon atoms were calculated geometrically (C–H= 0.96 Å). All H atoms were refined using a riding model and their isotropic displacement parameters were given a value 20% higher than the isotropic equivalent for the atom to which the H atoms were attached. The absolute structure of the crystals was assumed from the known absolute configuration of (*R*,*R*)-1,2-diaminocyclohexane used in synthesis. A Mercury[35] program was used to prepare the drawings.

Atomic coordinates and displacement parameters for **2a** have been deposited at the Cambridge Crystallographic Data Center (CCDC) and allocated the deposition number CCDC 29,2051.

6. Computational details

Geometry optimizations were performed with the use of b3lyp hybrid functional and split-valence 6-31g(d) basis set.[36] For all structures, frequency calculations were carried out at the b3lyp/6-31g(d) level of theory to establish that the conformations are stable. In our computations all excited-state calculations have been performed based upon the ground state geometries of single molecules with the use of a Gaussian program package and semiempirical ZINDO/S method.[36] Thus the results correspond to vertical transitions, and the excitation energies can be compared with the band maxima in the experimental spectra. Rotatory strengths were calculated using length and velocity representations. In the present study the differences between the length and velocity calculated values of rotatory strengths were quite small, thus only velocity representations were taken under further considerations. The CD spectra were simulated by overlapping Gaussian functions for each transition according to the procedure described by Grimme and Diedrich.[37] No correlation for the medium dielectric constant was implemented.

All conformers of triads **1a**–**1c**, **2a**–**2c** are of C_2 symmetry.

Acknowledgements

We thank Dr. B. Nowak-Wydra for running some of the NMR experiments. This work was supported by the Committee of Scientific Investigations, grants no. 3T 09A 183 27 (to M.K.) and 4T 09A 185 25 (to U.R.). All calculations were performed at Poznań Supercomputing and Networking Center.

Supplementary data

Supplementary data associated with this article can be found in the online version, at doi:10.1016/j.tet.2006.05.039.

References and notes

1. Werz, D. B.; Seeberger, P. H. *Chem.—Eur. J.* **2005**, *11*, 3194–3206.
2. Rowan, A. E.; Nolte, R. J. M. *Angew. Chem., Int. Ed.* **1998**, *37*, 63–68.
3. Schmuck, C. *Angew. Chem., Int. Ed.* **2003**, *42*, 2448–2452.
4. Green, M. M.; Park, J.-W.; Sato, T.; Teramoto, A.; Lifson, S.; Selinger, R. L. B.; Selinger, J. V. *Angew. Chem., Int. Ed.* **1999**, *38*, 3138–3154.
5. Gellman, S. H. *Acc. Chem. Res.* **1998**, *31*, 173–180.
6. Hill, D. J.; Mio, M. J.; Prince, R. B.; Hughes, T. S.; Moore, J. S. *Chem. Rev.* **2001**, *101*, 3893–4011.
7. Sanford, A. R.; Yamato, K.; Yang, X.; Yuan, L.; Han, Y.; Gong, B. *Eur. J. Biochem.* **2004**, *271*, 1416–1425.
8. Huc, B. *Eur. J. Org. Chem.* **2004**, 17–29.
9. Berl, V.; Huc, I.; Khoury, R. G.; Lehn, J.-M. *Chem.—Eur. J.* **2001**, *7*, 2798–2809.
10. (a) Huc, I.; Maurizot, V.; Gornitzka, H.; Léger, J.-M. *Chem. Commun.* **2002**, 578–579; (b) Dolain, C.; Maurizot, V.; Huc, I. *Angew. Chem., Int. Ed.* **2003**, *42*, 2738–2740; (c) Dolain, C.; Maurizot, V.; Huc, I. *J. Am. Chem. Soc.* **2004**, *126*, 10049–10052.
11. Masu, H.; Sakai, M.; Kishikawa, K.; Yamamoto, M.; Yamaguchi, K.; Kohmoto, S. *J. Org. Chem.* **2005**, *70*, 1423–1431.
12. Hamuro, Y.; Geib, S. J.; Hamilton, A. D. *J. Am. Chem. Soc.* **1996**, *118*, 7529–7541.
13. (a) Appella, D. H.; Christianson, L. A.; Karle, I. L.; Powell, D. R.; Gellman, S. H. *J. Am. Chem. Soc.* **1996**, *118*, 13071–13072; (b) Krauthäuser, S.; Christianson, L. A.; Powell, D. R.; Gellman, S. H. *J. Am. Chem. Soc.* **1997**, *119*, 11719–11720; (c) Appella, D. H.; Christianson, L. A.; Klein, D. A.; Powell, D. R.; Huang, X.; Barchi, J. J.; Gellman, S. H. *Nature* **1997**, *387*, 381–384; (d) Applequist, J.; Bode, K. A.; Appella, D. H.; Christianson, L. A.; Gellman, S. H. *J. Am. Chem. Soc.* **1998**, *120*, 4891–4892; (e) Appella, D. H.; Christianson, L. A.; Karle, I. L.; Powell, D. R.; Gellman, S. H. *J. Am. Chem. Soc.* **1999**, *121*, 6206–6212; (f) Wang, X.; Espinosa, J. F.; Gellman, S. H. *J. Am. Chem. Soc.* **2000**, *122*, 4821–4822; (g) Porter, E. A.; Wang, X.; Lee, H.-S.; Weisblum, B.; Gellman, S. H. *Nature* **2000**, *404*, 565; (h) Porter, E. A.; Weisblum, B.; Gellman, S. H. *J. Am. Chem. Soc.* **2002**, *124*, 7324–7330; (i) Arnold, U.; Hinderaker, M. P.; Nilsson, B. L.; Huck, B. R.; Gellman, S. H.; Raines, R. T. *J. Am. Chem. Soc.* **2002**, *124*, 8522–8523; (j) Raguse, T. L.; Porter, E. A.; Weisblum, B.; Gellman, S. H. *J. Am. Chem. Soc.* **2002**, *124*, 12774–12785.
14. (a) Seebach, D.; Overhand, M.; Kühnle, F. N. M.; Martinoni, B. *Helv. Chim. Acta* **1996**, *79*, 913–941; (b) Seebach, D.; Ciceri, P. E.; Overhand, M.; Jaun, B.; Rigo, D.; Oberer, L.; Hommel, U.; Amstutz, R.; Widmer, H. *Helv. Chim. Acta* **1996**, *79*, 2043–2066; (c) Seebach, D.; Oberer, L.; Hommel, U.;

Widmer, H. *Helv. Chim. Acta* **1997**, *80*, 2033–2038; (d) Seebach, D.; Matthews, J. L. *Chem. Commun.* **1997**, 2015–2022; (e) Seebach, D.; Abele, S.; Gademann, K.; Guichard, G.; Hintermann, T.; Jaun, B.; Matthews, J. L.; Schreiber, J.; Oberer, L.; Hommel, U.; Widmer, H. *Helv. Chim. Acta* **1998**, *81*, 932–982; (f) Seebach, D.; Abele, S.; Sifferlen, T.; Hänggi, M.; Gruner, S.; Seiler, P. *Helv. Chim. Acta* **1998**, *81*, 2218–2243; (g) Werder, M.; Hauser, H.; Abele, S.; Seebach, D. *Helv. Chim. Acta* **1999**, *82*, 1774–1783; (h) Gademann, K.; Kimmerlin, T.; Hoyer, D.; Seebach, D. *J. Med. Chem.* **2001**, *44*, 2460–2468.

15. (a) Hamuro, Y.; Schneider, J. P.; DeGrado, W. F. *J. Am. Chem. Soc.* **1999**, *121*, 12200–12201; (b) Liu, D.; DeGrado, W. F. *J. Am. Chem. Soc.* **2001**, *123*, 7553–7559.
16. Archer, E. A.; Gong, H.; Krische, M. J. *Tetrahedron* **2001**, *57*, 1139–1159.
17. Gong, B.; Zeng, H. Q.; Zhu, J.; Yua, L. H.; Han, Y. H.; Cheng, S. Z.; Furukawa, M.; Parra, R. D.; Kovalevsky, A. Y.; Mills, J. L.; Skrzypczak-Jankun, E.; Martinovic, S.; Smith, R. D.; Zheng, C.; Szyperski, T.; Zeng, X. C. *Proc. Natl. Acad. Sci. U.S.A.* **2002**, *99*, 11583–11588.
18. (a) Bassani, D. M.; Lehn, J.-M.; Baum, G.; Fenske, D. *Angew. Chem., Int. Ed.* **1997**, *36*, 1845–1847; (b) Ohkita, M.; Lehn, J.-M.; Baum, G.; Fenske, D. *Chem.—Eur. J.* **1999**, *5*, 3471–3481; (c) Cuccia, L. A.; Lehn, J.-M.; Homo, J.-C.; Schmutz, M. *Angew. Chem., Int. Ed.* **2000**, *39*, 233–237; (d) Gardinier, K. M.; Khoury, R. G.; Khoury, J.-M.; Lehn, J.-M. *Chem.—Eur. J.* **2000**, *6*, 4124–4131; (e) Petitjean, A.; Cuccia, L. A.; Lehn, J.-M.; Nierengarten, H.; Schmutz, M. *Angew. Chem., Int. Ed.* **2002**, *41*, 1195–1198; (f) Cuccia, L. A.; Ruiz, E.; Lehn, J.-M.; Homo, J.-C.; Schmutz, M. *Chem.—Eur. J.* **2002**, *8*, 3448–3457.
19. (a) Brunsveld, L.; Prince, R. B.; Meijer, E. W.; Moore, J. S. *Org. Lett.* **2000**, *2*, 1525–1528; (b) Kübel, C.; Mio, M. J.; Moore, J. S.; Martin, D. C. *J. Am. Chem. Soc.* **2002**, *124*, 8605–8610; (c) Matsuda, K.; Stone, M. T.; Moore, J. S. *J. Am. Chem. Soc.* **2002**, *124*, 11836–11837; (d) Stone, M. T.; Moore, J. S. *Org. Lett.* **2004**, *6*, 469–472; (e) Heemstra, J. M.; Moore, J. S. *Org. Lett.* **2004**, *6*, 659–662; (f) Goto, H.; Heemstra, J. M.; Hill, D. J.; Moore, J. S. *Org. Lett.* **2004**, *6*, 889–892.
20. (a) Gin, M. S.; Yokozawa, T.; Prince, R. B.; Moore, J. S. *J. Am. Chem. Soc.* **1999**, *121*, 2643–2644; (b) Prince, R. B.; Brunsveld, L.; Meijer, E. W.; Moore, J. S. *Angew. Chem., Int. Ed.* **2000**, *39*, 228–230; (c) Lahiri, S.; Thompson, J. L.; Moore, J. S. *J. Am. Chem. Soc.* **2000**, *122*, 11315–11319; (d) Hill, D. J.; Moore, J. S. *Proc. Natl. Acad. Sci. U.S.A.* **2002**, *99*, 5053–5057; (e) Stone, M. T.; Fox, J. M.; Moore, J. S. *Org. Lett.* **2004**, *6*, 3317–3320.
21. (a) Tamatani, A.; Mio, M. J.; Moore, J. S. *J. Am. Chem. Soc.* **2001**, *123*, 1792–1793; (b) Tanatani, A.; Hughes, T. S.; Moore, J. S. *Angew. Chem., Int. Ed.* **2002**, *41*, 325–328; (c) Goto, K.; Moore, J. S. *Org. Lett.* **2005**, *7*, 1683–1686.
22. Lokey, R. S.; Iverson, B. L. *Nature* **1995**, *375*, 303–305.
23. Gawroński, J.; Gawrońska, K.; Grajewski, J.; Kacprzak, K.; Rychlewska, U. *Chem. Commun.* **2002**, 582–583.
24. (a) Elmer, S. P.; Pande, V. *J. Phys. Chem. B* **2001**, *105*, 482–485; (b) Elmer, S. P.; Pande, V. *J. Chem. Phys.* **2004**, *121*, 12760–12771; (c) Elmer, S. P.; Pande, V. *J. Chem. Phys.* **2005**, *122*, 124908; (d) Elmer, S. P.; Park, S.; Pane, V. S. *J. Chem. Phys.* **2005**, *123*, 114902.
25. Kaik, M.; Gawroński, J. *Tetrahedron: Asymmetry* **2003**, *14*, 1559–1563.
26. Gawroński, J.; Brzostowska, M.; Kacprzak, K.; Kołbon, H.; Skowronek, P. *Chirality* **2000**, *12*, 263–268.
27. (a) Gawroński, J.; Kaźmierczak, F.; Gawrońska, K.; Rychlewska, U.; Nordén, B.; Holmén, A. *J. Am. Chem. Soc.* **1998**, *120*, 12083–12091; (b) Gawroński, J.; Gawrońska, P.; Skowronek, K.; Holmén, A. *J. Org. Chem.* **1999**, *64*, 234–241.
28. Gawroński, J.; Kacprzak, K. *Chirality* **2002**, *14*, 689–702.
29. Speak, A. L. *Acta Crystallogr.* **1990**, *A46*, 194–201.
30. Allen, F. H. *Acta Crystallogr.* **2002**, *B58*, 380–388.
31. *CrystAlis CCD software*; Oxford Diffraction: Oxfordshire (England), 2000; Version 1.166.
32. Sheldrick, G. M. *Acta Crystallogr.* **1990**, *A46*, 467–473.
33. Sheldrick, G. M. *SHELXS-97, Program for the Solution of Crystal Structure*; University of Gottingen: Germany, 1997.
34. Sheldrick, G. M. *SHELXL-97, Program for the Refinement of Crystal Structure*; University of Gottingen: Germany, 1997.
35. (a) Bruno, I. J.; Cole, J. C.; Edgington, P. R.; Kessler, M. K.; Macrae, C. F.; McCabe, P.; Pearson, J.; Taylor, R. *Acta Crystallogr.* **2002**, *B58*, 389–397; (b) Taylor, R.; Macrae, C. F. *Acta Crystallogr.* **2001**, *B57*, 815–827.
36. Frisch, M. J.; Trucks, G. W.; Schlegel, H. B.; Scuseria, G. E.; Robb, M. A.; Cheeseman, J. R.; Zakrzewski, V. G.; Montgomery, J. A., Jr.; Stratmann, R. E.; Burant, J. C.; Dapprich, S.; Millam, J. M.; Daniels, A. D.; Kudin, K. N.; Strain, M. C.; Farkas, O.; Tomasi, J.; Barone, V.; Cossi, M.; Cammi, R.; Mennucci, B.; Pomelli, C.; Adamo, C.; Clifford, S.; Ochterski, J.; Petersson, G. A.; Ayala, P. Y.; Cui, Q.; Morokuma, K.; Salvador, P.; Dannenberg, J. J.; Malick, D. K.; Rabuck, A. D.; Raghavachari, K.; Foresman, J. B.; Cioslowski, J.; Ortiz, J. V.; Baboul, A. G.; Stefanov, B. B.; Liu, G.; Liashenko, A.; Piskorz, P.; Komaromi, I.; Gomperts, R.; Martin, R. L.; Fox, D. J.; Keith, T.; Al-Laham, M. A.; Peng, C. Y.; Nanayakkara, A.; Challacombe, M.; Gill, P. M. W.; Johnson, B.; Chen, W.; Wong, M. W.; Andres, J. L.; Gonzalez, C.; Head-Gordon, M.; Replogle, E. S.; Pople, J. A. *Gaussian 03*; Gaussian: Pittsburgh PA, 2001.
37. Diedrich, C.; Grimme, S. *J. Phys. Chem. A* **2003**, *107*, 2524–2539.